Hydrophobization of arabinoxylan with n-butyl glycidyl ether yields stretchable thermoplastic materials

International Journal of Biological Macromolecules 188 (2021) 491–500

Contents lists available at ScienceDirect

International Journal of Biological Macromolecules

journal homepage: www.elsevier.com/locate/ijbiomac

Hydrophobization of arabinoxylan with n-butyl glycidyl ether yields stretchable thermoplastic materials

Parveen Kumar Deralia [a,*], Aline Maire du Poset [b], Anja Lund [b], Anette Larsson [b], Anna Ström [b], Gunnar Westman [a,*]

[a] Chemistry and Biochemistry, Department of Chemistry and Chemical Engineering, Chalmers University of Technology, Kemivägen 10, SE-41296 Gothenburg, Sweden
[b] Applied Chemistry, Department of Chemistry and Chemical Engineering, Chalmers University of Technology, Kemivägen 10, SE- Gothenburg, Sweden

ARTICLE INFO

Keywords:
Arabinoxylan
One-step synthesis
Melt compression
Renewable biomass
Thermoplastic

ABSTRACT

Hemicelluloses are regarded as one of the first candidates for the development of value-added materials due to their renewability, abundance, and functionality. However, because most hemicelluloses are brittle, they can only be processed as a solution and cannot be processed using industrial melt-based polymer processing techniques. In this study, arabinoxylan (AX) was hydrophobized by incorporating butyl glycidyl ether (BuGE) into the hydroxyl groups through the opening of the BuGE epoxide ring, yielding alkoxy alcohols with terminal ethers. The formed BuGE derivatives were melt processable and can be manufactured into stretchable thermoplastic films through compression molding, which has never been done before with hemicellulose modified in a single step. The structural and thermomechanical properties of the one-step synthesis approach were compared to those of a two-step synthesis with a pre-activation step to demonstrate its robustness. The strain at break for the one-step synthesized AX thermoplastic with 3 mol of BuGE is ≈200%. These findings suggest that thermoplastic polymers can be composited with hemicelluloses or that thermoplastic polymers made entirely of hemicelluloses can be designed as packaging and stretchable electronics supports.

1. Introduction

Products derived from renewable and plant-based resources, as opposed to fossil resources, support and contribute to a more sustainable and bio-based economy. Renewable plant-based polymers such as cellulose, starch, and lignin have been at the forefront of their conversion to a variety of value-added products due to their appealing functionality and abundance. Depending on their biological origin and method of isolation, biopolymers have varying reactive and functional moieties in their structures. To compete with fossil resources-based refineries, the next generation of biorefineries must maximize feedstock value. Hemicellulose, the second most common plant-based polysaccharide polymer after cellulose, has not been pursued for materials in the same way that cellulose and starch have. It is most commonly used as a low-cost energy source, incinerated with lignin, and used for animal feed or, to a lesser extent, materials.

In recent decades, many studies have been conducted to investigate hemicelluloses for a variety of applications, such as films, coatings, emulsions, additives, and hydrogels in materials [1–5] and stretchable substrates in electronic devices [6,7]. Arabinoxylans (AX) are hemicelluloses found in cereal grains with a beta-1,4-linked xylopyranosyl backbone and side groups such as arabinofuranosyl, arabino-linked feruloyl esters, and glucuronosyl residues [8,9]. AX is more water soluble than xylan due to its high arabinofuranosyl side chains [10,11]. Because of strong intramolecular and/or intermolecular interactions, polysaccharides become brittle, limiting their use in packaging and stretchable electronics applications.

From an industrial standpoint, thermoplastic biopolymers are preferred due to their suitability for industrial processing techniques, lower time-intensive processing, and low solvent requirements, allowing for fast and scalable manufacturing.

Due to tighter intra- and/or intermolecular interactions in polysaccharides, their glass transition temperatures (T_g) are high and are greater than 200 °C which is close to their degradation temperatures [12,13]. This makes melt processing difficult to perform due to the inaccessible melt phase [14]. To overcome this, plasticizers are used to alter the molecular interactions in starch [15,16] and cellulose acetate [17] to allow melt processing. Polysaccharides were chemically

* Corresponding authors.
E-mail addresses: deralia.parveen@gmail.com (P.K. Deralia), westman@chalmers.se (G. Westman).

https://doi.org/10.1016/j.ijbiomac.2021.08.041
Received 30 May 2021; Received in revised form 14 July 2021; Accepted 5 August 2021
Available online 10 August 2021

modified to overcome weak mechanical properties, plasticizer migration problems, and recrystallization over time [18–20].

Chemical modification of starch [21–24], proteins [25,26] and cellulose acetate [27–29] has been shown to improve processability and product performance. Several studies have been conducted to investigate the role of the structure and composition of arabinoxylan, as well as the degree of oxidation, in its processability and properties [30–32]. While several other studies have focused on changing the structure of xylan to decrease inherent hydrophilicity through acetylation [30,33], propylene oxide [32,34], butyl glycidyl ether [35,36] and periodate oxidation [37], with only a few of these reducing Tg [32,35,37]. Despite significant success in broadening the material application spectrum through solvent processing of hemicelluloses, the majority of these hemicellulose-derived materials lack stretchability, let alone practical application, and melt processability.

Previous research has shown that ring opening polymerization of ε-caprolactone on hemicellulose can make it melt processable with and without hydrophobization [38,39]. A recent study used an alkylketene dimer and an alkenyl succinic anhydride to hydrophobize xylan, but thermoplasticity was not obtained [40]. These studies used DMSO-based reaction systems. We previously demonstrated that arabinoxylans etherified with n-butyl glycidyl ether (BuGE) using water as a solvent can be molded by melt compression to produce stretchable thermoplastic films after successive periodate oxidation and reduction (activation) [31,41]. It was discovered that AX melt processing can be accomplished in two steps (activation and etherification). We also showed that the structure and composition of native AX and modified AX, as well as the structure, chemical and physical properties of the etherification agents, all have a significant impact on the thermal processability and thermomechanical properties of the resulting materials [41]. AX with an arabinosyl-to-xylosyl ratio of 1.1 was suitable for compression molding, but had only 25% elongation when modified with 5 mol of n-butyl glycidyl ether [31]. The initial argument for the above study was that ring opening oxidation would increase the flexibility of the arabino groups and thus promote thermoplasticity. We envisage that by reducing the strength of the intermolecular noncovalent interactions while keeping the hydrophobicity of the biopolymers, it may be possible to increase the stretchability on the macroscale and the bulk properties while still maintaining the thermal processability.

In this paper, we present a one-step hydrophobization of arabinoxylan with n-butyl glycidyl ether to produce thermoplastic materials and evaluate their melt processability and thermomechanical properties using a melt compression molding process. Additionally, AX was activated (in a range of low to high ring opening oxidation and subsequent reduction; Table 1) before incorporating n-butyl glycidyl ether. The purpose of this two-step synthesis was to investigate how the hydroxyl groups in native AX and activated AX influence the melt processability and thermomechanical properties in the case of one-step and two-step synthesized materials. To determine the robustness of the one-step synthesis, we compared the structures and thermomechanical properties of the one-step and two-step synthesized materials.

2. Experimental

2.1. Reagents and materials

All chemicals, reagents, enzymes, and solvents were purchased from Sigma-Aldrich (Schnelldorf, Germany) or Fisher Scientific (Sweden) with the exception of ethanol, which was purchased from Solveco AB (Sweden). Throughout, distilled water was used. The dialysis tube (Spectra/Por®, MWCO 3500) was provided by Spectrum Laboratories Inc., CA, USA. Wheat bran (WB) supplied by Lantmännen AB (Stockholm, Sweden) was used as received (dry matter 91%) for arabinoxylan extraction. With minor modifications, arabinoxylan (AX) was extracted from wheat bran according to the previous literature [42] (details in the Supplementary Material). The chemical composition of WB was determined using the standard National Renewable Energy Laboratory (NREL) method [43]: glucan 29 ± 2%, mannan 1 ± 0%, galactan 1.0 ± 0%, xylan 15 ± 1%, arabinan 10 ± 1%, acid insoluble lignin (AIL) 12 ± 2%, and ash 5% ± 0.0 (the rest, 27%, includes proteins, extractives, etc.). The extracted AX has the following chemical composition: glucan 7.5 ± 0.1%, xylan 35.2 ± 0.5%, arabinan 28.1 ± 0.4%, with an arabinosyl to xylosyl unit ratio (Araf/Xylp) of 0.8 and a molar mass of 212 kDa. The purity of the extracted AX is 72.2 ± 1.1%, with the remainder consisting of salts, lignin, and proteins and was used for etherification reactions without further purification. The experimental approaches to the synthesized materials in one and two steps are shown in Fig. 1a.

Table 1
Data on periodate oxidation and n-butyl glycidyl ether modification from 1-step synthesized (E-AX) and 2-step synthesized (E-A-AX) samples.

Entry[a]	Sample[b]	PI/ASU[c], mole	Oxidation level 1[d], %	Oxidation level 2[e], %	NaOH & BuGE/ASU, mole
1	$E_{1.0}$AX	0	0	0	1
2	$E_{3.0}$AX	0	0	0	3
3	$E_{5.0}$AX	0	0	0	5
4	$E_{1.0}A_{8\%}$AX	0.10	8	7	1
5	$E_{3.0}A_{8\%}$AX	0.10	8	7	3
6	$E_{1.0}A_{20\%}$AX	0.25	20	24	1
7	$E_{3.0}A_{20\%}$AX	0.25	20	24	3
8	$E_{3.0}A_{31\%}$AX	0.35	31	28	3
9	$E_{5.0}A_{31\%}$AX	0.35	31	28	5
10	$E_{3.0}A_{49\%}$AX	0.50	49	39	3
11	$E_{5.0}A_{49\%}$AX	0.50	49	39	5

[a] Entry 1–3 and 4–11 are synthesized samples in 1 step and 2 step.
[b] E and A denote the mole equivalence of BuGE and activation level which are subscripted.
[c] Mole of periodate (PI) per anhydrous sugar unit (ASU, pentose and hexose), the reduction reaction parameters were similar for all reactions.
[d] Periodate consumption determined by UV–Vis (see Eq. 1 in the Supplementary Material).
[e] Based on the difference in the pre- and post-activation monosaccharide content (see Eq. 2 in the Supplementary Material).

2.2. Synthesis

2.2.1. Arabinoxylan activation

Arabinoxylan was activated through a series of periodate ring opening oxidation and reduction reactions (Table 1 and Fig. 1b-(i)). Periodate oxidation was carried out according to the published literature [44,45]. AX (4 g dry basis, 30.30 mmol) and 10 ml of 2-propanol in 165 ml of H_2O were added to a glass bottle with a screw cap and a stir bar, and the mixture was stirred at 50 °C for 1 h. The oxidation reaction was carried out in the dark at room temperature (20 °C) for 14 h after adding sodium meta periodate dissolved in 25 ml of H_2O at a concentration of 2% (Table 1). After 14 h, 2 g of sodium borohydride $NaBH_4$ and 0.3 g of sodium monophosphate NaH_2PO_4 were slowly added to the reaction mixture in 50 ml of H_2O, producing a reaction concentration of 1.6%. For 4 h, the reduction was carried out at 20 °C. Following the completion of the reduction, 300 ml of a 2:1 methanol/diethyl ether mixture was poured into the reaction content to precipitate the product. After centrifugation, the product, activated AX (A-AX), was recovered and used for the etherification reaction without drying.

2.2.2. Synthesis of arabinoxylan ether and activated arabinoxylan ether

Activated AX (A-AX) and AX were etherified (Fig. 1b-(ii)) according to the reported literature [35] with some changes. A glass bottle with a stir bar was filled with activated AX (A-AX from the activation step) or AX (4 g dry basis, 30.30 mmol) and 60 ml of H_2O, and the mixture was stirred at 50 °C for 1 h. After being cooled to room temperature, an aqueous NaOH solution (different NaOH of 45 ml-Table 1) was added and stirred at 20 °C for an additional 1 h. After adding dropwise n-butyl glycidyl ether (BuGE) for 30 min at 45 °C, the etherification reaction was

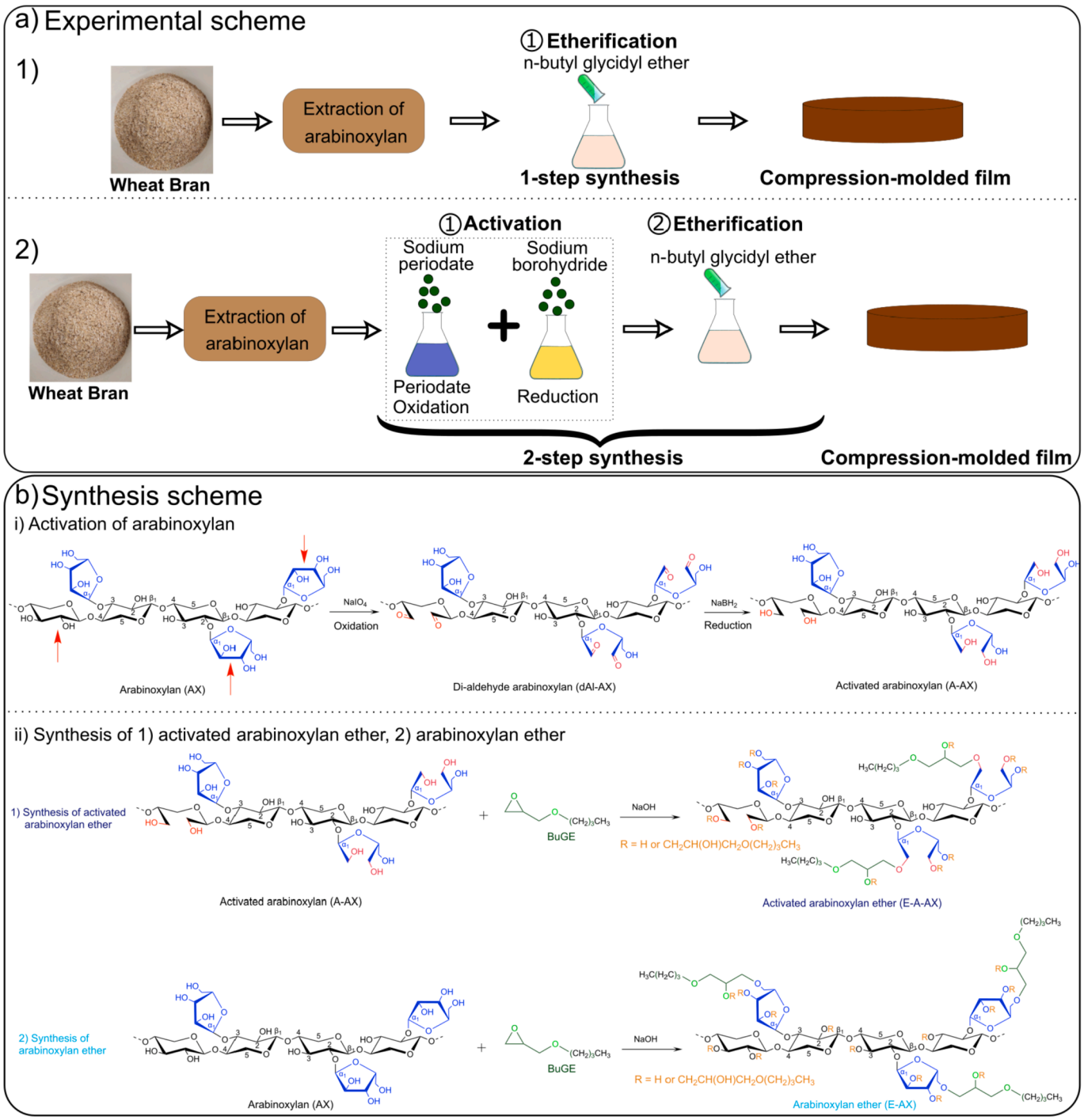

Fig. 1. a) Simplistic experimental steps for 1) one-step and 2) two-step synthesized materials; b) Synthesis scheme of i) activation achieved by successive periodate oxidation and reduction and ii) production of activated AX ether (1) and AX ether (2).

carried out for 16 h (Table 1). After cooling, the mixture was neutralized to pH 7.0 with 2 M CH_3COOH. To precipitate the product, 150 ml of a 1:0.7 methanol/diethyl ether mixture was added to the reaction. After centrifugation, the product was recovered and dried under a vacuum at room temperature for 14 h. Tables S1-S3 and S5 show the chemical and physical properties of BuGE, as well as sample coding and final product yields.

2.3. Film fabrication

The films were fabricated using melt compression molding and solvent casting processes (Table S5). To compress mold, the sample was cut into small pieces to obtain a homogeneous melt and placed in a die set with dimensions of 80 × 80 × 0.5 or 50 × 50 × 0.5 mm (L x W x T) between two metal plates (150 °C) with no pressure for 3 min. The mold was compressed (50 kPa) at 140 °C for 4 min after heating to obtain a film of 0.4 mm thick. The samples were dissolved in H_2O or an ethanol water mixture (3:1, ethanol 95%) at 20 g/L for casting and stirred for 1 h at 50 °C. After it was cooled, the solution was poured into a Petri dish and dried at room temperature.

2.4. Characterization

The level of oxidation in the activated AX samples was determined by measuring a) periodate consumption using UV-spectroscopy and b) sugar content before and after activation using monosaccharide quantification with HPLC. Additional information can be found in the Supplementary Material.

Samples were hydrolyzed in two stages with sulfuric acid using the NREL procedure [43]. A 1 ml aliquot of the hydrolyzed sample was used for carbohydrate analysis, while the remainder was neutralized and lyophilized before being used for NMR analysis. HPLC and NMR were used to determine the substitution of n-butyl glycidyl ether (Eqs. 3 and 5 in the Supplementary Material). Solubilized monosaccharides were quantified using a Dionex ICS-4000 HPAEC system equipped with PAD (both from Dionex, Sunnyvale, CA, USA) and a Dionex CarboPac PA1 analytical column.

At 25 °C, a Varian MR-400 MHz spectrometer (Agilent Technologies) was used to collect ^{1}H nuclear magnetic resonance (NMR) spectra. Solubilized freeze-dried monosaccharide samples were dissolved in D_2O for 1 h at 50 °C.

ATR–FTIR measurements were performed on a PerkinElmer Frontier FT-IR spectrometer (Waltham, MA) equipped with an ATR accessory. Before measurement, the room-temperature dried samples were conditioned for 24 h at 23 °C and 50% RH. In a typical measurement, 128 scans with a resolution of 2 cm^{-1} between 400 and 4000 cm^{-1} were averaged. Spectrum software was used to correct the baselines of the spectra and Origin Pro 2018 was used to plot them.

Gel permeation chromatography (GPC) was used to measure the number average molecular weight (M_n), weight-average molecular weight (M_w), and polydispersity index ($Đ = M_w / M_n$) using an integrated system PL-GPC 50 equipped with RI and UV detectors (Polymer Laboratories, Varian Inc.) set at $\lambda = 280$ nm and a series-coupled Polar Gel-M column with a guard column (300 × 7.5 mm2 and 50 × 7.5 mm2, 8 μm). DMSO/LiBr (10 mM) was used as an eluent (0.5 ml/min). Samples were made by dissolving 2 mg/ml of polymer in the eluent and then filtering through 0.2 m syringe filters. Pullulan standards were used to calibrate the system (180–708,000 Da).

To investigate the phase transition, a differential scanning calorimetry (DSC) measurement (Mettler Toledo DSC2 calorimeter equipped with an HSS7 sensor and a TC-125MT intercooler) with a heating and cooling rate of 10 °C/min was used. In the sealed aluminum pan, 5 mg of sample were placed. As a reference, standard aluminum pans and lids were sealed. For neat AX, A-AX, and *E*-A-AX samples, a heating/cooling/heating procedure was used in a temperature range of 30 to 250 °C and − 100 to 230 °C. T_g was chosen as the inflection point of the endotherm transition in the second heating cycle after analyzing two samples of each material. Figs. S11-S18 show representative DSC heating-cooling-heating cycle curves and second heating curves highlighted by the endothermic transition.

A Q800 DMA was used to measure dynamic mechanical properties (TA Instruments). In dynamic tension mode, rectangular specimens with dimensions of 30 mm in length and 6 mm in width and thicknesses of 0.4 mm cut from compression-molded films or 0.1 mm cut from solution-cast film were measured. Measurements were made at a heating rate of 3 °C/min and a frequency of 1 Hz, with a strain of 0.02%.

Thermal stability was measured using a TGA / DSC 3 + Star System (Mettler Toledo, Columbus, OH, USA) with a nitrogen flow of 50 ml / min. In an aluminum pan, 5 mg of sample was placed and scanned from 20 to 500 °C at a ramp rate of 5 °C/min.

Tensile specimens were prepared using compression molding or solvent casting, as described in the film fabrication section. The rectangular samples were 20 × 5.6 mm and 0.1 and 0.4 mm thick for the compression-molded and solvent-cast samples, respectively. They were air dried and conditioned for 24 h at 23 °C and 50% RH before being measured. The mechanical properties of the samples were measured at room temperature with an Instron 5565A instrument (Norwood, MA, USA) at 30 mm/min and a 100 N load cell. The results were based on an average of 4–5 measurements.

3. Results and discussion

Fig. 1b shows the synthesis scheme. A series of thermoplastic materials was synthesized in neat AX using 1, 3, and 5 mol of BuGE to obtain thermoplastic materials in a single step (Entries 1, 2, and 3 in Table 1; Fig. 1b-ii part 2). In the case of two-step synthesized thermoplastic materials, AX was first activated at levels of 8%, 20%, 31% and 49%, and then 1, 3, 5 mol of BuGE were mixed into the four activated AXs to produce eight different samples (Entries 4–11 in Table 1). In the case of one-step synthesis, the possible reaction sites for etherification reactions are the native hydroxyl groups of sugar units (Arabinan, xylan [Fig. 1b-ii part 1] and glucan [not shown]; also shown in Fig. S1c, both in the xylosyl units in the backbone [orange alkoxide unit] and arabinosyl side units [light green alkoxide unit]; Fig. S1c) and the hydroxyl groups of the alkoxide moieties (red alkoxide unit in Fig. S1c). However, in the case of two-step synthesis, there are additional reaction sites in the form of hydroxyl groups formed after pre-activation in the backbone and arabinosyl side units (Fig. 1b-ii part 1 or Fig. S1d). BuGE molar substitution (MS) in the samples was measured using ^{1}H NMR (Fig. 2a and Fig. S7). This method measures all possible substitutions of BuGE.

The general trend is that MS increases with the amount of BuGE alone (one-step synthesis) and with the combination of activation level and amount of BuGE (two-step synthesis). The MS of the synthesized samples of 1 step ($E_{1.0}AX = 0.45$) and 2 step ($E_{1.0}A_{8\%}AX = 0.41$, $E_{1.0}A_{20\%}AX = 0.39$) does not change significantly (Fig. 2a) at 1 mol BuGE. At 3 mol of BuGE, the MS of the one-step synthesized sample ($E_{3.0}AX = 3.64$) is lower than that of the two-step.

synthesized samples ($E_{3.0}A_{8\%}AX = 2.18$, $E_{3.0}A_{20\%}AX = 2.05$, $E_{3.0}A_{31\%}AX = 1.87$, $E_{3.0}A_{49\%}AX = 3.32$) [Fig. 2a]. The MS of the synthesized sample in one step ($E_{5.0}AX = 6.70$) at 5 mol of BuGE is greater than that of the 31% activated sample ($E_{5.0}A_{31\%}AX = 4.78$), but comparable to that of the 49% activated sample ($E_{5.0}A_{49\%}AX = 6.73$). The MS data show that an increase in the activation level does not change the MS with the same amount of BuGE when comparing the synthesized samples in 1 and 2 steps. In other words, the one-step and two-step approaches yield a similar molar substitution (MS).

FTIR analysis further supports the structural evolution of the samples following BuGE. Fig. 2c shows representative annotated spectra of activated AX, neat AX, 1-step, and 2-step synthesized samples, and Fig. S9 shows the complete set of spectra for each category. The following observations support the incorporation of BuGE in activated AX and AX samples: Enhancement and shift of OH stretching centered at 3300 cm^{-1} to the left due to disruption of inter and/or intramolecular interactions (Fig. 2c and Fig. S9-d); appearance of new peaks representing CH stretching (3000–2850 cm^{-1}) and bending [46,47] (between 1500 and 1350 cm^{-1}) and CH_2 rocking (740 cm^{-1}).

The presence of a long-chain linear aliphatic structure can be seen in the new peak at 740 cm^{-1} (CH_2 rocking vibration) and its counterpart at 1465 cm^{-1} (stronger CH_2 vibration) [47]. These findings show that the etherification reactions of the one- and two-step synthesis reactions were successful and are consistent with the MS data discussed above.

When BuGE is attached to the hydroxyl group of a sugar unit (arabinosyl, xylosyl and glucosyl), the resulting unit, that is, a sugar unit with an alkoxide terminal, is no longer a monosaccharide and will not be detected as a monosaccharide in carbohydrate analysis of etherified samples. Therefore, if we do carbohydrate analysis on the samples before and after etherification with HPLC, we can calculate the BuGE substitutions occurring on the sugar units. Note that ^{1}H NMR MS values include substitutions of all possible reaction sites, as discussed in the NMR section above. Carbohydrate units (pentose and hexose) that have not been affected by the pre-activation step in the case of two-step synthesis and have reacted with BuGE, as well as BuGE-reacted carbohydrate units in the case of one-step synthesis, are termed intact

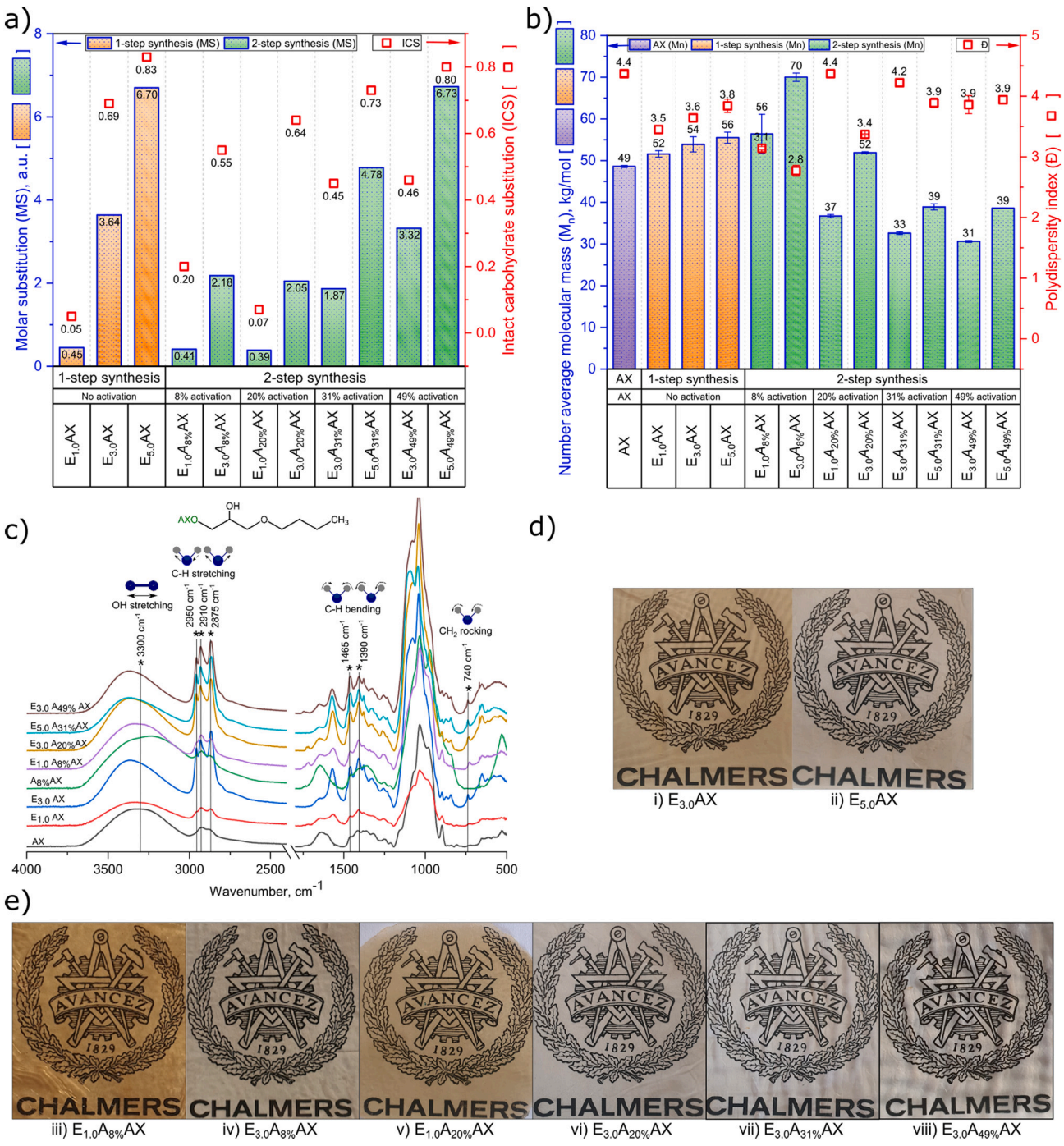

Fig. 2. a) ^{1}H NMR determined the molar substitution [left y-axis] and HPLC determined the intact carbohydrate substitution (ICS) [right y-axis] of the samples. Table S7 summarizes the MS and ICS values, with calculation details in the Supplementary Material; b) GPC determined the number average molecular masses (M_n) [left y-axis] and the polydispersity indices (Đ) [right y-axis] of the samples. Table S7 contains the values of M_n, Mw and Đ (M_w/M_n) values; c) FTIR spectrum of neat AX and representative spectra of *E*-AX, A-AX and E-A-AX sample series. Fig. S6 shows all spectra; d) melt compression-molded films of AX ether materials. $E_{1.0}$AX not shown because it was not thermally processable; e) melt compression-molded films of activated AX ether materials. The $E_{5.0}A_{31\%}$AX and $E_{5.0}A_{49\%}$AX films are not shown because they were not freestanding. The melt compression molding was performed at a temperature of 140 °C and a pressure of 50 kPa. Chalmers University of Technology (CTH) granted permission to use and does not claim ownership. The CTH logo is only used to determine the transparency of the film.

carbohydrate substitutions (ICS). Thus, ICS represents the fraction of sugar units whose OH groups were substituted with BuGE monomers (Eq. 3 and Fig. S1), and measures BuGE substitutions occurring only on sugar units. ICS results are shown in Fig. 2a. The ICS values increase with increasing numbers of BuGE monomers alone and with increasing activation levels and the number of BuGE monomers combined. At 3 mol of BuGE, the ICS of $E_{3.0}$AX (0.69) is higher than that of the A-AX samples activated at different levels (0.55, 0.45, 0.46, except 0.64 for $E_{3.0}A_{20\%}$AX). At 5 mol of BuGE, the ICS of $E_{5.0}$AX (0.83) is slightly higher than that of 2-step synthesized samples ($E_{5.0}A_{31\%}$AX = 0.73, $E_{5.0}A_{49\%}$AX = 0.80). This demonstrates that the opening of the ring occurring during pre-activation has an effect on the efficiency of the BuGE substitution. Using 5 mol of BuGE resulted in a sticky product and sticky films for activated AX ethers.

Fig. 2b shows the average molar masses and polydispersity indices of neat AX, AX ether, and activated AX ether, which are also listed in Table S7. Figs. S3-S5 show the molar mass distribution (MWD) curves. Note that our molar masses are relative (not absolute) to the linear Pullulan standard used in this study. The M_n and M_w of neat AX are similar to wheat AX (low viscosity) in a previous study using DMSO as a solvent [10], but lower than in another study [37]. Compared to water-based SEC, DMSO-based SEC (used in this study) has lower mean molar masses [10]. The molar mass distributions shown in Figs. S3–S5 exhibit multimodal peaks. Figs. S6–8 show the deconvoluted peaks corresponding to multiple polymer fractions. The population fractions of these polymer fractions are given in Table S8. There are two major polymeric fractions (peak 1 and 3) in all samples, with two minor fractions (peak 2 and 4) [Table S8 and Figs. S6–8]. The shape of the molar mass distribution (MWD) of AX ethers synthesized in one step tails toward a higher molar mass (Fig. S3b, c, and d) with an increase in the amount of BuGE compared to the MWD of neat AX (Fig. S3a). With an increase in BuGE moles, the M_ns of the AX ethers increase (49 to 56 kDa) (Fig. 2b).

However, this tailing toward a higher molar mass phenomenon is not observed in the two-step synthesized samples (Figs. S4 and S5). Activation in the two-step synthesis includes periodate oxidation, which has been shown to reduce the molar weight due to polymer degradation [37,48]. Even after BuGE is incorporated, the M_ns of activated AX ethers (M_n = 33, 39, 31, and 39) with 31% activation are lower than those of neat AX (M_n = 49 kDa). This also lends credence to the notion that periodate oxidation degrades the polymer [37,48]. The molar masses of activated AX ethers with activation of 8% and 20% activation (M_n = 56, 70, 52 kDa, except for $E_{1.0}A_{20\%}AX$ M_n = 37 kDa) are higher than those of neat AX (M_n = 49 kDa), and MWD are narrower, as evidenced by lower polydispersity indices.

Melt compression molding is a common technique used in industrial polymer processing. Melt processing has advantages in terms of sustainability and cost because it requires less solvent/no solvent and less energy than solvent processing. Melt compression molding was used to process the AX ether and A-AX ether samples, and the resulting films are shown in Fig. 2d-e. With the exception of the $E_{1.0}AX$ sample, both the one-step and two-step synthesized samples could be melt processed. Furthermore, at room temperature, the activated AX ethers of $E_{5.0}A_{31\%}AX$ and $E_{5.0}A_{49\%}AX$ were already very soft and could not form free-standing films (not shown in Fig. 2). This behavior can be explained by two factors: 1) degradation when 31% and 49% activation are used; and 2) the use of 5 mol of BuGE results in the introduction of BuGE to ring-opened carbohydrate units, as evidenced by the ICS and MS data (Fig. 2a). In other words, these samples lack rigidity due to the lower number of intact xylosyl units in the structure of the backbone (see xylan data in Fig. S2c and Table S6 for $E_{5.0}A_{31\%}AX$ and $E_{5.0}A_{49\%}AX$) compared to the one-step synthesized sample ($E_{5.0}AX$) with the same mole of BuGE and a rigid xylan backbone with all intact xylosyl units (Fig. S2b and Table S6) with attached BuGE. The yellow-brown color difference in films may be due to protein and starch carbohydrates [49,50].

Differential scanning calorimetry (DSC) was used to determine the glass transition temperature (T_g) (Fig. 3 and listed in Table S10). Figs. S11-S18 show examples of thermograms. The T_g of activated AX (A-AX) is between 180 and 201 °C for all activation levels (8–49%), which is comparable to the T_g of neat AX (189 ± 3 °C) [Fig. 3].

These findings are consistent with those of a previous study [37]. There are two types of samples: a) samples with a single distinct endotherm/Tg, such as $E_{1.0}AX$, $E_{1.0}A_{8\%}AX$,and $E_{1.0}A_{20\%}AX$; and b) samples with two distinct endotherms/T_g (one subzero and one above zero), such as $E_{3.0}AX$, $E_{5.0}AX$, $E_{3.0}A_{8\%}AX$, $E_{3.0}A_{20\%}AX$, $E_{3.0}A_{31\%}AX$, $E_{5.0}A_{31\%}AX$, $E_{3.0}A_{49\%}AX$ and $E_{5.0}A_{49\%}AX$ (Fig. 3 and Table S10). We also performed a dynamic mechanical analysis of the materials to confirm the calorimetric results.

In comparison to DSC, DMA is more sensitive to the registering of molecular relaxations and thermal transitions because it applies

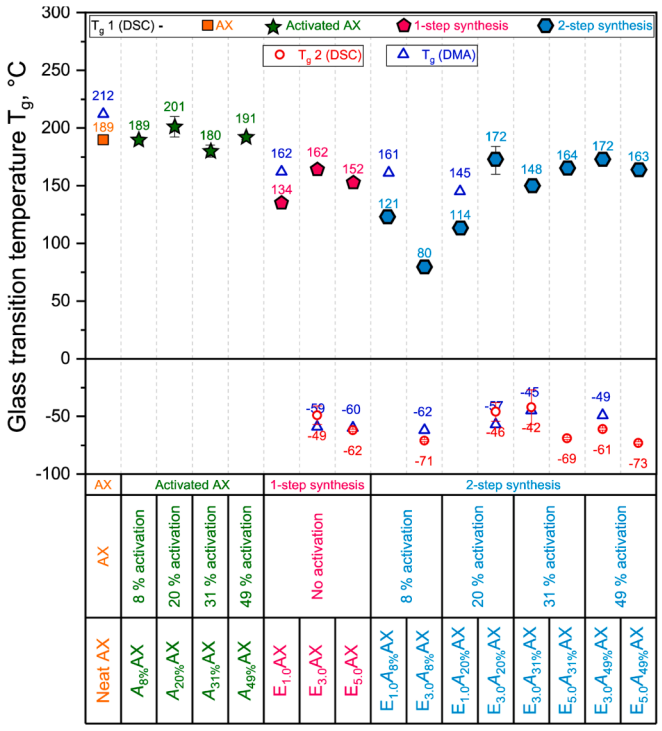

Fig. 3. DSC and DMA determined glass transition temperatures (T_gs) of the neat AX, activated AX, and one- and two-step synthesized samples. T_gs are also listed in Table S10. T_g1 and T_g2 are the DSC-based above-zero endotherm and subzero endothermic transitions, respectively. Tg (DSC) are the mean (n = 2) of the second heating scan and are measured as inflection points of the DSC endotherms. T_gs (DMA) are the peaks of the loss modulus (E") curves. DMA-based T_gs are not available for activated AX and two activated AX ethers ($E_{5.0}A_{31\%}AX$ and $E_{5.0}A_{31\%}AX$) because the films were very brittle for the former samples and soft for the latter samples.

mechanical stress to the sample while varying the temperature. The DMA results confirmed subzero transitions in $E_{3.0}AX$, $E_{5.0}AX$, $E_{3.0}A_{8\%}AX$, $E_{3.0}A_{20\%}AX$, $E_{3.0}A_{31\%}AX$ and $E_{3.0}A_{49\%}AX$ (Fig. 4a-f and Table S10). Because these materials soften after their first glass transition, DMA was unable to register the second glass transition above zero (Fig. 4a-f). Fig. 3 shows the T_gs of the loss modulus peaks. Fig. 4 a-j and Figs. S16–17 show the DMA curves.

The thermal transition of the first cluster samples ($E_{1.0}AX$, $E_{1.0}A_{8\%}AX$,and $E_{1.0}A_{20\%}AX$) may be caused by the xylan backbone and/or the polymer without extended side chains in the form of a long alkoxide carbon chain of the open epoxide-ring BuGE moiety. The MS substitution data (Fig. 2a; MS = 0.40) of these samples already show few extended side chains. In the case of two-Tg regime samples, subzero T_g could be attributed to longer alkoxide side chains, while the second T_g could be attributed to a xylan backbone with fewer substituted parts. These claims are supported by the appearance of a new peak in the FTIR spectra of 740 cm^{-1} (CH_2 rocking vibration; Fig. 2c) indicating a long-chain linear aliphatic structure [47] and higher MS values determined by ^1H NMR (Fig. 2a). These findings are consistent with the dual T_g properties of multiblock synthetic polymers [51,52], conjugated polymers [53], etherified arabinoxylan [41] and esterified cellulose [54].

Thermogravimetric analysis (TGA) was performed to evaluate the thermal stability. Figs. S21–23 show TGA profiles of one-step degradation for all samples. The characteristic parameters of thermal degradation include the temperatures at different % mass losses and the amount of final residue (char) formed at 500 °C (FR). These values are summarized in Table 2. We observe that the thermal stability of activated AX samples increases with increasing activation level (Table 2 and Fig. S21a and a'). However, the thermal stability decreases upon the introduction

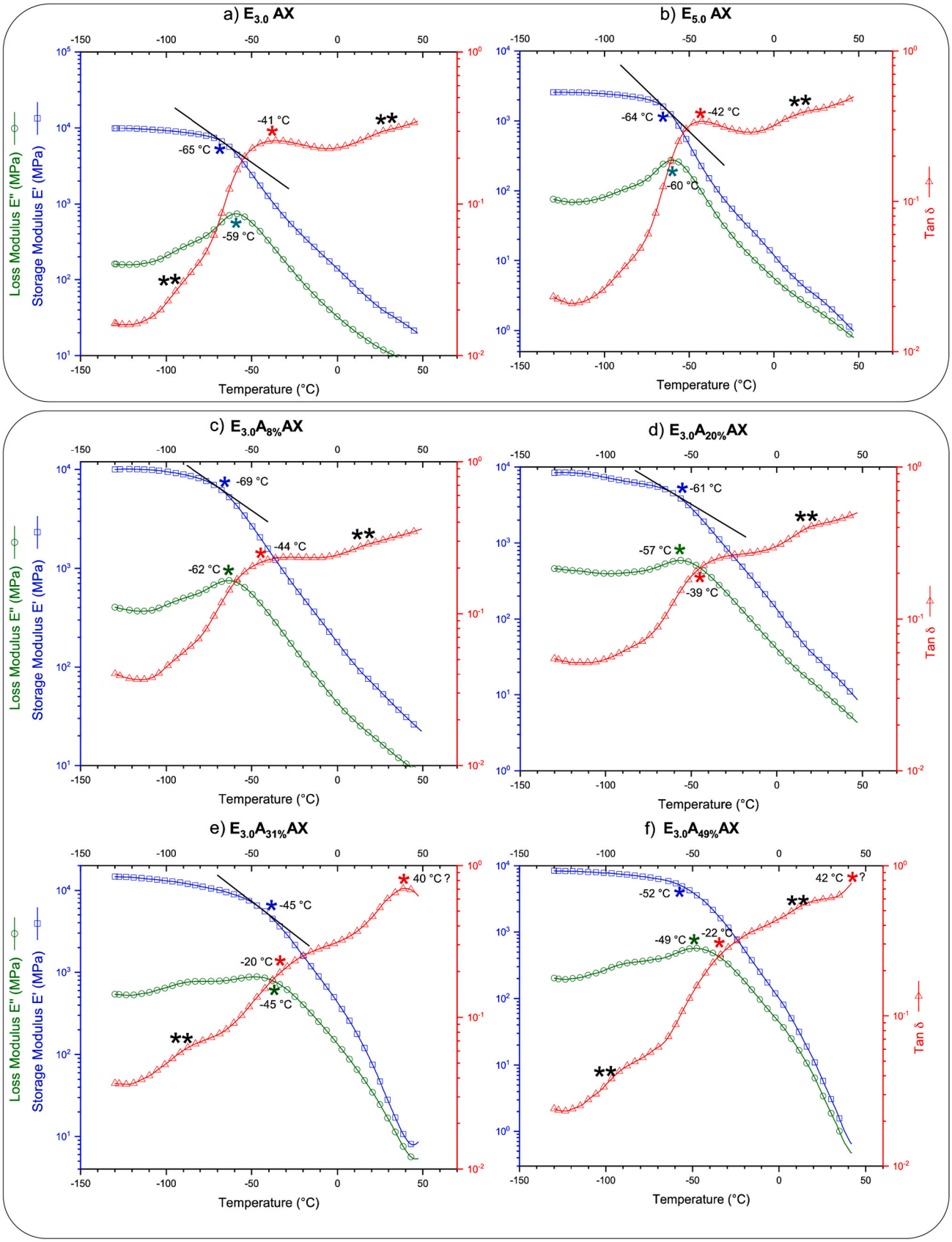

Fig. 4. DMA curves showing the storage modulus, loss modulus, and Tan δ evolution with respect to temperature of a) $E_{3.0}AX$, b) $E_{5.0}AX$, c) $E_{3.0}A_{8\%}AX$, d) $E_{3.0}A_{20\%}AX$, e) $E_{3.0}A_{31\%}AX$ and f) $E_{3.0}A_{49\%}AX$. A single star* indicates the T_g corresponding to each curve. The double star sign** on the Tan δ profile marks the presence of minor thermal transitions. DMA tests were performed with a dynamic strain of 0.02% at a frequency of 1 Hz with a heating rate of 3 °C/min.

Table 2
Uniaxial tensile and thermogravimetric analysis (TGA) data of neat AX activated AX samples, the 1-step synthesized samples (E-AX) and 2-step synthesized samples (E-A- AX).

Entry	Sample	E, MPa	σ_t, MPa	ε_b, %	T_{onset}, °C	$T_{inflection}$, °C	T_{endset}, °C	Final Residue, %
1	Neat AX	2125 (92)	43.7 (12.0)	3.4 (1)	256 (8)	278 (7)	299 (5)	27 (2)
2	A8% AX	–	–	–	266 (2)	280 (0)	293 (2)	40 (1)
3	A20% AX	–	–	–	268 (2)	285 (1)	301 (0)	42 (2)
4	A31% AX	–	–	–	270 (1)	288 (1)	304 (0)	43 (0)
5	A49% AX	–	–	–	274 (1)	289 (1)	319 (2)	41 (1)
6	E1.0 AX	1535 (65)	42.6 (8.2)	8.2 (2)	258 (1)	292 (3)	314 (0)	25 (0)
7	E3.0 AX	5 (1.1)	2.7 (0.4)	200 (35)	183 (13)	252 (26)	313 (0)	16 (0)
8	E5.0 AX	1 (0.4)	0.6 (0.2)	239 (21)	189 (2)	227 (9)	267 (5)	11 (1)
9	E1.0 A8% AX	1316 (131)	46 (2.4)	16.9 (4)	263 (*)	293 (*)	311 (*)	26 (*)
10	E3.0 A8% AX	27 (6.1)	5.3 (0.6)	142 (12)	209 (9)	286 (4)	313 (2)	17 (0)
11	E1.0 A20% AX	1445 (70)	46.6 (1.8)	19.2 (2)	263 (*)	296 (*)	317 (*)	25 (*)
12	E3.0 A20% AX	1 (0.2)	1.2 (0.3)	246 (34)	238 (2)	292 (2)	317 (1)	18 (1)
13	E3.0 A31% AX	1 (0.1)	0.1 (0.0)	309 (51)	220 (3)	300 (1)	324 (1)	16 (1)
14	E5.0 A31% AX	n.d.	n.d.	n.d.	214 (0)	246 (2)	322 (2)	11 (0)
15	E3.0 A49% AX	7 (1.6)	0.7 (0.1)	134 (29)	154 (1)	289 (6)	317 (2)	17 (0)
16	E5.0 A49% AX	n.d.	n.d.	n.d.	188 (*)	251 (*)	312 (*)	10 (*)

Entry 1, 2–5, 6–8 and 9–16 are neat AX, activated AX, 1-step synthesized, and 2-step synthesized samples. Tensile and thermogravimetric data are the mean of 5 and 2 measurements. Standard deviations are in parentheses. E Young's modulus, σ_t max tensile stress, ε_b tensile strain at break. Entry 1–5 and 6–16 are solvent-cast and compression-molded films. Solvent-cast films were too fragile/brittle for tensile measurement. n.d. could not be determined because the film was not free-standing, Tonset initial degradation temperature, Tinflection temperature at the maximum degradation rate, Tendset final degradation temperature, final residue (FR)- char content at 500 °C. * Data from one replication.

of BuGE monomers in the AX ethers and the activated AX ethers, as reflected from the reduction in the onset degradation temperature (T_{onset}) compared to those of their parent counterparts (Neat AX and activated AX). This can be attributed to the presence of alkoxide chains after the opening of the epoxide ring on the OH groups of the polymers. The endset degradation temperatures (T_{endset}) of the AX ether and the activated AX ethers are higher than those of their parent counterparts. This behavior of decrease in T_{onset} and increase in T_{endset} can be explained due to the presence of two phases, i.e., soft and hard phases, as evidenced by the DSC and DMA results above. These results are consistent with previous studies showing that lower temperatures of thermal degradation occurred after chemical modifications of cellulose [55] and arabinoxylan [31,37].

Fig. 5a and b show representative stress-strain curves of AX ether and A-AX ether samples, and Table 2 summarizes the elastic modulus (E), maximum tensile stress (σ_t), and elongation at break (ε_b). Due to the presence of the xylan backbone and side groups with a low molar substitution part, the elastic modulus (E) of neat AX, AX ether and activated AX samples with 1 mol BuGE (entries 1, 6, 9 and 11 in Table 2) is higher than those of other samples. The elastic modulus (E) of the remaining samples (entries 7, 8, 10, 12, 13, and 15 in Table 2) is lower than that of the samples mentioned above because of the formation of segments with longer alkoxide side chains with greater molar substitution after the introduction of BuGE into the polymer. Furthermore, as measured by elongation at break (for examples ε_b = 200, 239, 142, 246, 309 and 134%), these samples are more stretchable.

The stretchability of the one-step synthesized samples (Entries 7 = 200 ± 35 and 8 = 239 ± 21 in Table 2) is very similar to that of the two-step synthesized samples (Entries 12 and 13 = 246 ± 34 and 309 ± 51 in Table 2). This shows that increasing the activation level in conjunction with the amount of BuGE does not result in a proportional increase in stretchability. The increase in stretchability among the samples is due to an increase in intramolecular interactions and a decrease in intermolecular interactions. The former is caused by the presence of an oxygen atom in the alkoxide chain, which aids in coordination with the surrounding hydrogen atoms, while the latter is caused by the presence of

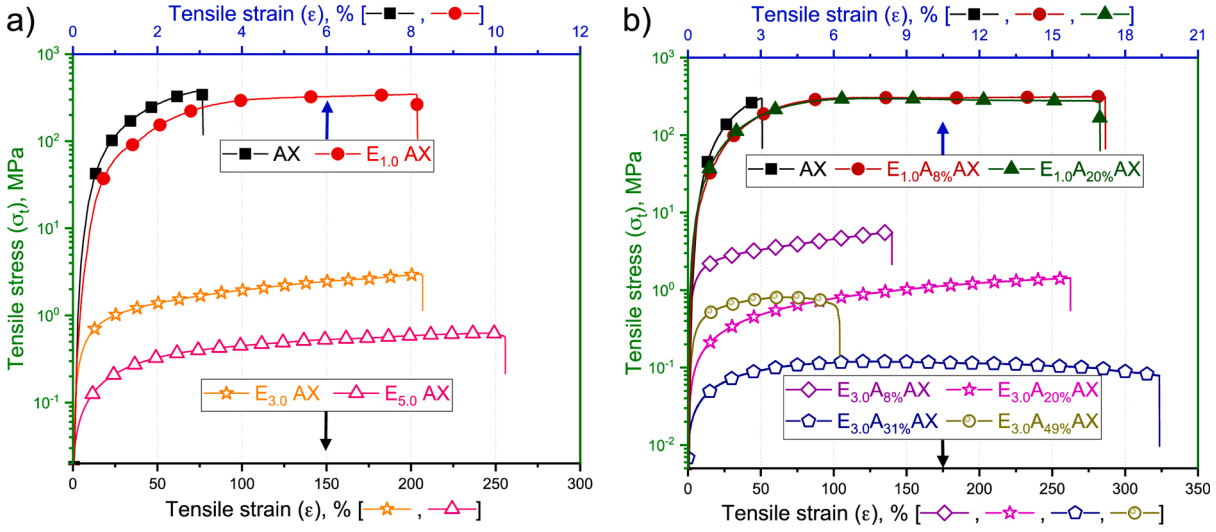

Fig. 5. Representative stress-strain curves of a) 1-step synthesized samples; b) 2-step synthesized samples. Data were obtained from the melt compression-molded films except for AX, $E_{1.0}$AX, $E_{1.0}A_{8\%}$AX and $E_{1.0}A_{20\%}$AX for which solvent-cast films were used. Sample fabrication is listed in Table S5. Tensile data are summarized in Table 2.

more interstitial space between chains. Intermolecular interactions are reduced, resulting in a decrease in E and an increase in ε_b.

AX ethers ($E_{3.0}AX$, $E_{5.0}AX$) and activated AX ethers ($E_{3.0}A_{8\%}AX$, $E_{3.0}A_{20\%}AX$, $E_{5.0}A_{31\%}AX$) have greater elongation (Table 2) and a narrower molar mass distribution (Figs. S3 c-d, S4 b and d and S5 b) compared to the other samples. This may be due to the fact that the narrowing of the MWD correlates with the stretchability of the polymer. With increasing incorporation of BuGE into neat AX and activated AX, an inverse relationship was observed between the elastic modulus and ε_b was observed. This finding is consistent with previous research, which found a similar phenomenon with increasing segment flexibility [56,57]. The E of the synthesized AX ethers in one step with higher molar mass fractions (tails toward MW, see Fig. S3 b-d) is greater than that of the synthesized samples in two steps with lower molar mass fractions (and have tailings of MWD toward LW; see Fig. S4 b and d). These findings indicate that polymers with tailings of the molar mass distribution oriented toward higher molar mass have higher E values than polymers with opposite tailing behavior in the MWD shape.

4. Conclusions

In conclusion, we demonstrated a new one-step strategy for the melt processing of AX via compression molding by hydrophobizing with BuGE. Previously, melt processing of AX was possible by pre-activating AX with successive periodate oxidation and reduction prior to BuGE hydrophobization. Except for the one with 1 mol BuGE, all hydrophobizing conditions resulted in melt processing. The thermomechanical properties of the synthesized samples in one and two steps were comparable. The highest elongation at break for a 1-step AX thermoplastic synthesized with 5 mol of BuGE was ≈239%.

The findings of this study not only provide a short path to biobased resources based on thermal processable and stretchable thermoplastics, but also provide new insights into the structure and thermomechanical properties of new biobased thermoplastics, which will be relevant for a broader scientific community working toward a better understanding of the structure-property relationships in hemicellulose and to expand the application areas for polysaccharide-based polymer.

CRediT authorship contribution statement

Parveen Kumar Deralia: Conceptualization, Methodology, Data curation, Formal analysis, Investigation, Visualization, Writing – original draft, Writing – review & editing. **Aline Maire du Poset:** Data curation, Investigation, Writing – review & editing. **Anja Lund:** Data curation, Investigation, Visualization, Writing – review & editing. **Anette Larsson:** Project administration, Funding acquisition, Visualization, Writing – review & editing. **Anna Ström:** Project administration, Funding acquisition, Visualization, Writing – review & editing. **Gunnar Westman:** Conceptualization, Methodology, Visualization, Project administration, Funding acquisition, Supervision, Writing – review & editing.

Declaration of competing interest

The authors state that they do not have any competing interests.

Acknowledgements

The authors are grateful for financial support from the Lantmännen Research Foundation, Stockholm, Sweden (Project/grant number 2017/H017). Drs. Hans Theliander and Merima Hasani provided access to the HPLC and GPC instruments, and Dr. Amit Kumar Sonker assisted with DSC experiments at Chalmers, Sweden.

Appendix A. Supplementary data

Supplementary data to this article can be found online at https://doi.org/10.1016/j.ijbiomac.2021.08.041.

References

[1] K.S. Mikkonen, M. Tenkanen, Sustainable food-packaging materials based on future biorefinery products: xylans and mannans, Trends Food Sci. Technol. 28 (2012) 90–102, https://doi.org/10.1016/j.tifs.2012.06.012.
[2] M.S. Lindblad, E. Ranucci, A.C. Albertsson, Biodegradable polymers from renewable sources. new hemicellulose-based hydrogels, Macromol. Rapid Commun. 22 (2001) 962–967, https://doi.org/10.1002/1521-3927(20010801)22:12<962::AID-MARC962>3.0.CO;2-E.
[3] K.S. Mikkonen, C. Xu, C. Berton-Carabin, K. Schroën, Spruce galactoglucomannans in rapeseed oil-in-water emulsions: efficient stabilization performance and structural partitioning, Food Hydrocoll. 52 (2016) 615–624, https://doi.org/10.1016/j.foodhyd.2015.08.009.
[4] K.S. Mikkonen, M. Tenkanen, P. Cooke, C. Xu, H. Rita, S. Willför, B. Holmbom, K. B. Hicks, M.P. Yadav, Mannans as stabilizers of oil-in-water beverage emulsions, LWT Food Sci. Technol. 42 (2009) 849–855, https://doi.org/10.1016/j.lwt.2008.11.010.
[5] D.U. Lima, R.C. Oliveira, M.S. Buckeridge, Seed storage hemicelluloses as wet-end additives in papermaking, Carbohydr. Polym. 52 (2003) 367–373, https://doi.org/10.1016/S0144-8617(03)00008-0.
[6] F. Hoeng, A. Denneulin, J. Bras, Use of nanocellulose in printed electronics: a review, Nanoscale 8 (2016) 13131–13154, https://doi.org/10.1039/c6nr03054h.
[7] Q. Fu, Y. Chen, M. Sorieul, Wood-based flexible electronics, ACS Appl. Mater. Interfaces 14 (2020) 3528–3538, https://doi.org/10.1021/acsnano.9b09817.
[8] M.E.F. Schooneveld-Bergmans, G. Beldman, A.G.J. Voragen, Structural features of (glucurono)arabinoxylans extracted from wheat bran by barium hydroxide, J. Cereal Sci. 29 (1999) 63–75, https://doi.org/10.1006/jcrs.1998.0222.
[9] M.S. Izydorczyk, J.E. Dexter, Barley ß-glucans and arabinoxylans: molecular structure, physicochemical properties, and uses in food products-a review, Food Res. Int. (2008), https://doi.org/10.1016/j.foodres.2008.04.001.
[10] L. Pitkänen, L. Virkki, M. Tenkanen, P. Tuomainen, Comprehensive multidetector HPSEC study on solution properties of cereal arabinoxylans in aqueous and DMSO solutions, Biomacromolecules 10 (2009) 1962–1969, https://doi.org/10.1021/bm9003767.
[11] M.J. Selig, L.G. Thygesen, C. Felby, E.R. Master, Debranching of soluble wheat arabinoxylan dramatically enhances recalcitrant binding to cellulose, Biotechnol. Lett. 37 (2015) 633–641, https://doi.org/10.1007/s10529-014-1705-0.
[12] J.L. Ren, R.C. Sun, C.F. Liu, Z.N. Cao, W. Luo, Acetylation of wheat straw hemicelluloses in ionic liquid using iodine as a catalyst, Carbohydr. Polym. (2007), https://doi.org/10.1016/j.carbpol.2007.04.022.
[13] A. Biswas, R.L. Shogren, J.L. Willett, Solvent-free process to esterify polysaccharides, Biomacromolecules 6 (2005) 1843–1845, https://doi.org/10.1021/bm0501757.
[14] L. Szczesniak, A. Rachocki, J. Tritt-Goc, Glass transition temperature and thermal decomposition of cellulose powder, Cellulose 15 (2008) 445–451, https://doi.org/10.1007/s10570-007-9192-2.
[15] L. Averous, E. Pollet, Nanobiocomposites based on plasticized starch, in: Starch Polym. From Genet. Eng. to Green Appl, 2014, pp. 211–239, https://doi.org/10.1016/B978-0-444-53730-0.00028-2.
[16] A.P. Mathew, A. Dufresne, Morphological investigation of nanocomposites from sorbitol plasticized starch and tunicin whiskers, Biomacromolecules (2002), https://doi.org/10.1021/bm0101769.
[17] S. Zepnik, S. Kabasci, R. Kopitzky, H.J. Radusch, T. Wodke, Extensional flow properties of externally plasticized cellulose acetate: influence of plasticizer content, Polymers (Basel) 5 (2013) 873–889, https://doi.org/10.3390/polym5030873.
[18] T. Mekonnen, P. Mussone, H. Khalil, D. Bressler, Progress in bio-based plastics and plasticizing modifications, J. Mater. Chem. A 1 (2013) 13379–13398, https://doi.org/10.1039/c3ta12555f.
[19] P. De Groote, J. Devaux, P. Godard, Effect of benzenesulfonamide plasticizers on the glass-transition temperature of semicrystalline polydodecamide, J. Polym. Sci. B Polym. Phys. 40 (2002) 2208–2218, https://doi.org/10.1002/polb.10281.
[20] Hongbo Li, Michel A. Huneault, Comparison of sorbitol and glycerol as plasticizers for thermoplastic starch in TPS/PLA blends, Rawal Med. J. 43 (2018) 483–485, https://doi.org/10.1002/app.
[21] A.L. Chaudhary, P.J. Torley, P.J. Halley, N. McCaffery, D.S. Chaudhary, Amylose content and chemical modification effects on thermoplastic starch from maize - processing and characterisation using conventional polymer equipment, Carbohydr. Polym. 78 (2009) 917–925, https://doi.org/10.1016/j.carbpol.2009.07.023.
[22] A.L. Chaudhary, M. Miler, P.J. Torley, P.A. Sopade, P.J. Halley, Amylose content and chemical modification effects on the extrusion of thermoplastic starch from maize, Carbohydr. Polym. 74 (2008) 907–913, https://doi.org/10.1016/j.carbpol.2008.05.017.
[23] B. Volkert, A. Lehmann, T. Greco, M.H. Nejad, A comparison of different synthesis routes for starch acetates and the resulting mechanical properties, Carbohydr. Polym. 79 (2010) 571–577, https://doi.org/10.1016/j.carbpol.2009.09.005.

[24] N. Reddy, Y. Yang, Preparation and properties of starch acetate fibers for potential tissue engineering applications, Biotechnol. Bioeng. 103 (2009) 1016–1022, https://doi.org/10.1002/bit.22331.
[25] A. Bhattacharya, B.N. Misra, Grafting: a versatile means to modify polymers: techniques, factors and applications, Prog. Polym. Sci. 29 (2004) 767–814, https://doi.org/10.1016/j.progpolymsci.2004.05.002.
[26] D. Xi, C. Yang, X. Liu, M. Chen, C. Sun, Y. Xu, Graft polymerization of styrene on soy protein isolate, J. Appl. Polym. Sci. 98 (2005) 1457–1461, https://doi.org/10.1002/app.22278.
[27] R. Quintana, O. Persenaire, L. Bonnaud, P. Dubois, Recent advances in (reactive) melt processing of cellulose acetate and related biodegradable bio-compositions, Polym. Chem. 3 (2012) 591–595, https://doi.org/10.1039/c1py00421b.
[28] G. Stiubianu, A. Nicolescu, A. Nistor, M. Cazacu, C. Varganici, B.C. Simionescu, Chemical modification of cellulose acetate by allylation and crosslinking with siloxane derivatives, Polym. Int. 61 (2012) 1115–1126, https://doi.org/10.1002/pi.4189.
[29] C.J. Biermann, J.B. Chung, R. Narayan, Grafting of polystyrene onto cellulose acetate by nucleophilic displacement of mesylate groups using the polystyrylcarboxylate anion, Macromolecules 20 (1987) 954–957, https://doi.org/10.1021/ma00171a010.
[30] A.M. Stepan, A. Höije, H.A. Schols, P. De Waard, P. Gatenholm, Arabinose content of arabinoxylans contributes to flexibility of acetylated arabinoxylan films, J. Appl. Polym. Sci. 125 (2012) 2348–2355, https://doi.org/10.1002/app.36458.
[31] M. Börjesson, G. Westman, A. Larsson, A. Ström, Thermoplastic and flexible films from arabinoxylan, ACS Appl. Polym. Mater. 1 (2019) 1443–1450, https://doi.org/10.1021/acsapm.9b00205.
[32] R.K. Jain, M. Sjöstedt, W.G. Glasser, Thermoplastic xylan derivatives with propylene oxide, Cellulose (2000), https://doi.org/10.1023/A:1009260415771.
[33] F.Z. Belmokaddem, C. Pinel, P. Huber, M. Petit-Conil, D.Da Silva Perez, Green synthesis of xylan hemicellulose esters, Carbohydr. Res. 346 (2011) 2896–2904, https://doi.org/10.1016/j.carres.2011.10.012.
[34] C. Laine, A. Harlin, J. Hartman, S. Hyvärinen, K. Kammiovirta, B. Krogerus, H. Pajari, H. Rautkoski, H. Setälä, J. Sievänen, J. Uotila, M. Vähä-Nissi, Hydroxyalkylated xylans - their synthesis and application in coatings for packaging and paper, Ind. Crop. Prod. 44 (2013) 692–704, https://doi.org/10.1016/j.indcrop.2012.08.033.
[35] T. Nypelö, C. Laine, M. Aoki, T. Tammelin, U. Henniges, Etherification of wood-based hemicelluloses for interfacial activity, Biomacromolecules 17 (2016) 1894–1901, https://doi.org/10.1021/acs.biomac.6b00355.
[36] M.S. Peresin, K. Kammiovirta, H. Setälä, T. Tammelin, Structural features and water interactions of etherified xylan thin films, J. Polym. Environ. 20 (2012) 895–904, https://doi.org/10.1007/s10924-012-0469-7.
[37] M. Börjesson, A. Larsson, G. Westman, A. Ström, Periodate oxidation of xylan-based hemicelluloses and its effect on their thermal properties, Carbohydr. Polym. 202 (2018) 280–287, https://doi.org/10.1016/j.carbpol.2018.08.110.
[38] A. Svärd, E. Brännvall, U. Edlund, Modified and thermoplastic rapeseed straw xylan: a renewable additive in PCL biocomposites, Ind. Crop. Prod. 119 (2018) 73–82, https://doi.org/10.1016/j.indcrop.2018.03.067.
[39] W. Farhat, R. Venditti, A. Ayoub, F. Prochazka, C. Fernández-de-Alba, N. Mignard, M. Taha, F. Becquart, Towards thermoplastic hemicellulose: chemistry and characteristics of poly-(e-caprolactone) grafting onto hemicellulose backbones, Mater. Des. 153 (2018) 298–307, https://doi.org/10.1016/j.matdes.2018.05.013.
[40] H.N. Cheng, A. Biswas, S. Kim, C.R. Alves, R.F. Furtado, Synthesis and characterization of hydrophobically modified xylans, Polymers (Basel) 13 (2021) 1–14, https://doi.org/10.3390/polym13020291.
[41] P.K. Deralia, A.M. Du Poset, A. Lund, A. Larsson, A. Strom, G. Westman, Oxidation level and glycidyl ether structure determine thermal processability and thermomechanical properties of arabinoxylan-derived thermoplastics, ACS Appl. Bio Mater. 4 (2021) 3133–3144, https://doi.org/10.1021/acsabm.0c01550.
[42] M. Börjesson, L. Härdelin, F. Nylander, K. Karlsson, A. Larsson, G. Westman, Arabinoxylan and nanocellulose from a kilogram-scale extraction of barley husk, Bioresources 13 (2018) 6201–6220, https://doi.org/10.15376/biores.13.3.6201-6220.
[43] A. Sluiter, B. Hames, R. Ruiz, C. Scarlata, J. Sluiter, D. Templeton, Determination of structural carbohydrates and lignin in biomass determination of structural carbohydrates and lignin in biomass, Natl. Renew. Energy Lab. 2011 (2010). NREL/TP-510-42618.
[44] M. Siller, H. Amer, M. Bacher, W. Roggenstein, T. Rosenau, A. Potthast, Effects of periodate oxidation on cellulose polymorphs, Cellulose 22 (2015) 2245–2261, https://doi.org/10.1007/s10570-015-0648-5.
[45] H. Amer, T. Nypelö, I. Sulaeva, M. Bacher, U. Henniges, A. Potthast, T. Rosenau, Synthesis and characterization of periodate-oxidized polysaccharides: dialdehyde xylan (DAX), Biomacromolecules 17 (2016) 2972–2980, https://doi.org/10.1021/acs.biomac.6b00777.
[46] J. Wang, P. Somasundaran, Mechanisms of ethyl(hydroxyethyl) cellulose-solid interaction: influence of hydrophobic modification, J. Colloid Interface Sci. (2006), https://doi.org/10.1016/j.jcis.2005.06.072.
[47] J. Coates, Interpretation of infrared spectra, a practical approach, Encycl. Anal. Chem. (2006), https://doi.org/10.1002/9780470027318.a5606.
[48] I.L. Andresen, T. Painter, O. Smidsrød, Concerning the effect of periodate oxidation upon the intrinsic viscosity of alginate, Carbohydr. Res. 59 (1977) 563–566, https://doi.org/10.1016/S0008-6215(00)83194-8.
[49] M. Krishna, C.I. Nindo, S.C. Min, Development of fish gelatin edible films using extrusion and compression molding, J. Food Eng. 108 (2012) 337–344, https://doi.org/10.1016/j.jfoodeng.2011.08.002.
[50] J.F. Martucci, R.A. Ruseckaite, Tensile properties, barrier properties, and biodegradation in soil of compression - molded gelatin-dialdehyde starch films, J. Appl. Polym. Sci. 112 (2009) 2166–2178, https://doi.org/10.1002/app.29695.
[51] M.T. Martello, D.K. Schneiderman, M.A. Hillmyer, Synthesis and melt processing of sustainable poly(e-decalactone)-block-poly(lactide) multiblock thermoplastic elastomers, ACS Sustain. Chem. Eng. 2 (2014) 2519–2526, https://doi.org/10.1021/sc500412a.
[52] J. Zhang, R. Deubler, M. Hartlieb, L. Martin, J. Tanaka, E. Patyukova, P. D. Topham, F.H. Schacher, S. Perrier, Evolution of microphase separation with variations of segments of sequence-controlled multiblock copolymers, Macromolecules 50 (2017) 7380–7387, https://doi.org/10.1021/acs.macromol.7b01831.
[53] A. Sharma, X. Pan, J.M. Bjuggren, D. Gedefaw, X. Xu, R. Kroon, E. Wang, J. A. Campbell, D.A. Lewis, M.R. Andersson, Probing the relationship between molecular structures, thermal transitions, and morphology in polymer semiconductors using a woven glass-mesh-based DMTA technique, Chem. Mater. 31 (2019) 6740–6749, https://doi.org/10.1021/acs.chemmater.9b01213.
[54] Z. Chen, J.J. Zhang, P. Xiao, W. Tian, J.J. Zhang, Novel thermoplastic cellulose esters containing bulky moieties and soft segments, ACS Sustain. Chem. Eng. 6 (2018) 4931–4939, https://doi.org/10.1021/acssuschemeng.7b04466.
[55] H. Fukuzumi, T. Saito, T. Iwata, Y. Kumamoto, A. Isogai, Transparent and high gas barrier films of cellulose nanofibers prepared by TEMPO-mediated oxidation, Biomacromolecules 10 (2009) 162–165, https://doi.org/10.1021/bm801065u.
[56] M. Abubekerov, J. Wei, K.R. Swartz, Z. Xie, Q. Pei, P.L. Diaconescu, Preparation of multiblock copolymers: via step-wise addition of l-lactide and trimethylene carbonate, Chem. Sci. 9 (2018) 2168–2178, https://doi.org/10.1039/c7sc04507g.
[57] W. Guerin, M. Helou, J.F. Carpentier, M. Slawinski, J.M. Brusson, S.M. Guillaume, Macromolecular engineering via ring-opening polymerization (1): L-lactide/trimethylene carbonate block copolymers as thermoplastic elastomers, Polym. Chem. 4 (2013) 1095–1106, https://doi.org/10.1039/c2py20859h.